IEEE Access
Multidisciplinary | Rapid Review | Open Access Journal

Received July 22, 2018, accepted August 25, 2018, date of publication September 5, 2018, date of current version September 28, 2018.

Digital Object Identifier 10.1109/ACCESS.2018.2868731

Total Variation and Rank-1 Constraint RPCA for Background Subtraction

JIZE XUE[1], YONGQIANG ZHAO[1], (Member, IEEE), WENZHI LIAO[2], (Senior Member, IEEE), AND JONATHAN CHEUNG-WAI CHAN[3]

[1]School of Automation, Northwestern Polytechnical University, Xi'an 710072, China
[2]Department of Telecommunications and Information Processing, Ghent University-TELIN-IMEC, 9000 Ghent, Belgium
[3]Department of Electronics and Informatics, Vrije Universiteit Brussel, 1050 Brussels, Belgium

Corresponding author: Yongqiang Zhao (zhaoyq@nwpu.edu.cn)

This work was supported in part by the National Natural Science Foundation of China under Grant 61771391 and Grant 61371152 and in part by the Fund for Scientific Research in Flanders (FWO) project data fusion for image analysis in remote sensing under Grant G037115N. The work of W. Liao was supported by the Research Foundation Flanders (FWO-Vlaanderen).

ABSTRACT Background subtraction (BS) in video sequences is a main research field, and the aim is to separate moving objects in the foreground from stationary background. Using the framework of schemes-based robust principal component analysis (RPCA), we propose a novel BS method employing the more refined prior representations for the static and dynamic components of the video sequences. Specifically, the rank-1 constraint is exploited to describe the strong low-rank property of background layer (temporal correlation of static component), and 3-D total variation measure and L_1 norm are used to model the spatial-temporal smoothness of foreground layer and sparseness of noise (dynamic component). This method introduces rank-1, smooth, and sparse properties into the RPCA framework for BS task, and it is dubbed TR1-RPCA. In addition, an efficient algorithm based on the alternating direction method of multipliers is designed to solve the proposed BS model. Extensive experiments on simulated and real videos demonstrate the superiority of the proposed method.

INDEX TERMS Background subtraction, total variation, rank-1 property, robust principal component analysis, spatial-temporal correlations.

I. INTRODUCTION

Background subtraction (BS) originates from many applications in computer vision and pattern recognition, including moving object detection [1], object tracking [2], video surveillance [3] and so on. This operation involves recovering a high quality background component from a given observation or video frames degraded by outliers. The algorithms used for modeling the static and dynamic components have great effects on the performance of BS. Recently, many BS methods have been proposed [4]–[12].

Among various BS modeling approaches, one of the most famous ones is pixel-based methods. Lin *et al.* [4] utilized a mixture of Gaussian probability density functions, i.e. Gaussian Mixture Models, to model color intensity variations of individual pixels, which can provide a tradeoff between robustness to background changes and sensitivity to foreground abnormalities. Li *et al.* [5] characterized background appearances under a Bayesian framework using features extracted over spectral-spatial-temporal domains and their statistics property. In [6], an alternative strategy to infer the pixels as either background or foreground is presented. By considering local pixel prior knowledge, the decision framework is based on maximum a posteriori Markov random field. Using a combination of a series of codebooks, Guo *et al.* [7] used hierarchical scheme and distance function to describe the pixel states across the background and the foreground. A major effect of codebook is to promote efficiency as data volume is reduced via compressed information. In [8] and [9], the self-organizing BS algorithms based on artificial neural network were used to detect moving objects.

Another type of popular BS methods is based on the robust principal component analysis (RPCA) [10], which decomposed a video into a single low-rank component and a sparse component, and therefore the background variations are modelled naturally as approximately low rank and foreground objects as sparse errors. Candes *et al.* [10] exploited the RPCA technique for BS problem by decomposing video sequences into a low-rank component denoting background

and a sparse component denoting foreground, which can be expressed as the following optimization problems.

$$\min_{L,E} \|L\|_* + \lambda\|E\|_1, \quad s.t.\ Y = L + E \tag{1}$$

where $Y \in \mathbb{R}^{mn\times t}$ is the observed video streams, mn and t are the size of a frame and the number of frames, respectively. L and E correspond to the background and foreground components. Due to the intrinsic relation of the background images over temporal domain, the reshaped matrix is of low-rankness ($\|L\|_*$ denotes the nuclear norm of matrix L). And the L_1-norm is employed to characterize the sparseness of the foreground. However, the model is performed for BS task under coarse assumption for static and dynamic components, which correspond to the video background and foreground respectively. Therefore, it is necessary to consider the finer knowledge to deal with the growing challenges.

Focusing on the limitations of the RPCA-based methods, in this paper, we propose a TV and rank-1 regularized RPCA model for BS, taking full advantage of the static and dynamic component prior information. Our contributions can be summarized as three folds: First, it is the first work to model the BS task in a rank-1 constraint RPCA framework. This rank-1 constraint RPCA-based video representation enables us to better encode the static component (i.e., latent background knowledge) of temporal structures in a video sequence. Second, we further refine the dynamic component in RPCA, it can be regarded as the superposition of smooth video foreground and sparse noise along the spatial-temporal domain, which can be described by total variation and L_1 norm terms. Third, we design efficient algorithms based on ADMM to solve the proposed model and achieve competitive performances with state-of-the-art methods based on various video sequences.

The paper is organized as follows: we provide an overview of related works about RPCA-based BS tasks in Section II. Then we introduce the TR1-RPCA model in Section III, specifically, the property analysis and modellings of static and dynamic components are presented in Sections III-A and III-B, and Section III-C describes the optimization algorithm to solve the TR1-RPCA. In Section III-IV we give the experiments results, and finally we present our conclusions in Section V.

II. RELATED WORKS

The main goal of BS is to separate the underlying low-rank and sparse components from its observation. As background and foreground layers of the data possess intrinsic low-rank and sparse structure, the RPCA framework has achieved a great success in BS problems. Comprehensive reviews can be found in [11] and [12], we will provide only a brief review for the current progress on this topic.

Considering that the underlying properties on background and foreground, some improved methods based on RPCA using joint spatial-temporal constraints have been proposed [10], [14], [15], [21]–[39]. As for the modelling of the low-rank component, the low-rank approximation based on the nuclear norm is biased, which may lead to an erroneous subspace estimation, especially in BS task, with the weak and even inaccurate low-rank constraint. In order to meliorate estimating bias of the nuclear norm, several recent studies investigated the use of some non-convex low-rank regularizers, such as the weighted nuclear norm [13], [14], Schatten p-norm [15]–[17], log function penalty [18], [19], capped norm [20] and fixed-rank-1 [21]. Extensive applications on image denoising, background subtraction and image inpainting have validated the effectiveness of non-convex low-rank representations. Low-rank matrix factorization (LRMF) is another representative approach utilizing low-rank presentation for BS [22]–[26]. Instead of using the sparse and low-rank components characterization in the original RPCA model, Zhao *et al.* [22] proposed a generalized RPCA model based on the Bayesian framework and treated noise errors as a mixture of Gaussians (MoG). The MoG can approximate various noises such as Laplacian, Gaussian, sparse noises and any mixtures of them, and LRMF is used to estimate the low-rank component. In the presence of outliers, robust LRMF methods have been proposed in [23], where a convex low-rank regularization for factorization matrix is introduced to improve the robustness of subspace learning, without considering too much extra prior information. To fit unknown noise distribution, which cannot be pure Gaussian (L_2 loss function) or Laplacian (L_1 loss function), Meng and De La Torre [24] proposed a LRMF problem with MoG noise to effectively deal with the problem of foreground modeling. Along with their previous works in [22] and [24], they proposed an online BS method with joint MoG and LRMF constraints [25], this model have a good generalization in other subspace learning tasks, including image alignment and video stabilization applications. Similar to [23], Wang *et al.* [26] adopt two nonconvex terms instead of the nuclear norm to approximate the rank function in RPCA model. Ebadi and Izquierdo [27] used the structured-sparsity of super-pixel to estimate dynamic foreground regions under the RPCA framework, so that the spatial coherence on these regions are considered. Sobral *et al.* [28] constrained the sparse component by shape prior and confidence maps from spatial saliency. Javed *et al.* [29]– [31] employed inter-intra frame graph Laplacian regularization to learn latent low-rank of the background part. Xu *et al.* [32] explored the global spatial compactness and the appearance consistency of the foreground for low-rank and sparse separation, which were characterized by the similar pixel pairs in neighbor and the informative graphs for the pixels.

In the above-mentioned works, the foreground component is encoded by sparse priors. In fact, other than the sparsity term, the TV term can also be used and could be more effective in modelling the spatial-temporal information of the video foreground. In [33]–[35], TV regularization is utilized to only depict the continuity of moving objects over the spatial domain, and subsequent works [36]–[39] have further generalized the spatial continuity of foreground component

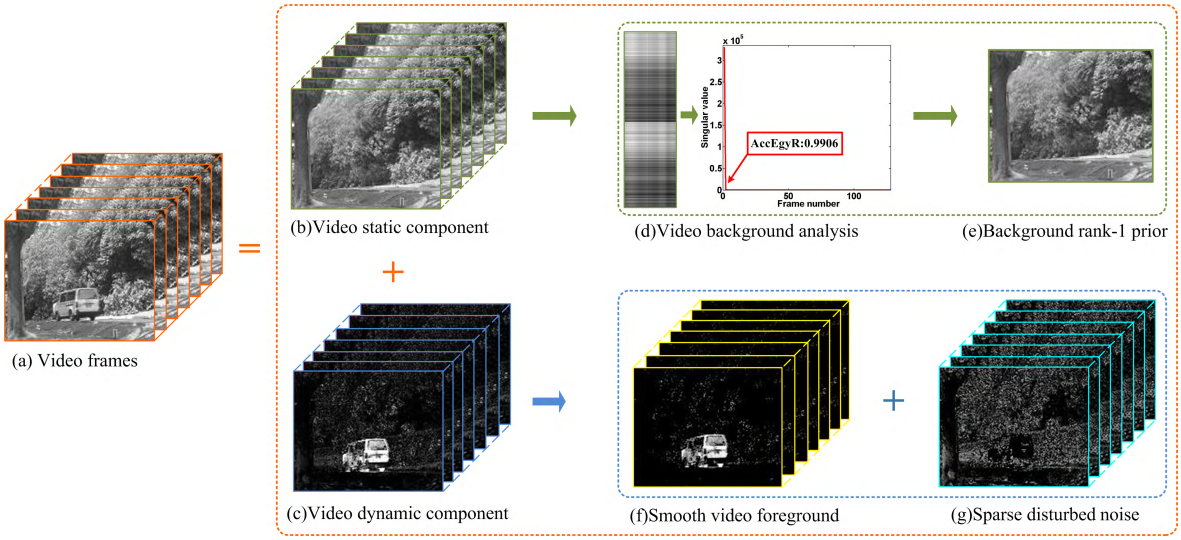

FIGURE 1. Illustration of video priors. (a) indicates original video, (b) and (c) are video static and dynamic components. (d) and (e) indicate the rank-1 prior information of video background (static component) based on the strong temporal correlation. (f) and (g) indicate the smoothness and sparseness prior information of the video dynamic components corresponding to foreground and noise descriptions.

to spatial-temporal continuity, namely the 3D-TV regularized RPCA framework for BS. However, those approaches neglect the finer structure of background and foreground over the spatial-temporal domain, and this lead to two shortcomings: (1) The nuclear norm and its revised version cannot reveal the nearly repetitive property underlying the video frames; (2) Superficial presentations are no longer effective to model the foreground where only the complex dynamic component is suitable.

Very recently, other authors have designed some real-time strategies for BS task, which speedup the algorithm by sub-matrices computation [40], compressive sampling [41], [42] or GPU implementations [43]. Another type of accelerated strategy is multiple online methods [25], [44]–[46], its core idea is to incrementally compute only one frame at a time, and gradually enhance the background estimation by each frame updating. The state-of-the-art approaches along this research line mainly include OPRMF [44], GRASTA [45], GOSUS [46], ReProcs [47], MEDRoP [48] and incPCP [49], [50]. The GRASTA and OPRMF employed based-L_1 norm loss function for each frame to encode sparse foreground component, and updated subspace via ADMM strategy. The GOSUS introduced a more complex loss term to characterize the structured sparsity of video foreground. Besides, the recently proposed PracReProCS, MEDRoP and incPCP are the incremental extensions of the classical PCP algorithm.

III. PROPOSED TR1-RPCA FOR BACKGROUND SUBTRACTION

In this section, we will present a novel TV and rank-1 regularized RPCA model for the BS task. First, we present our detailed analysis for video decomposition, focusing especially on the temporal correlations of static component spatial-temporal continuity and sparseness of dynamic component. Then, we leverage different component properties to build the BS model.

A. PROPERTY ANALYSIS AND MODELING STATIC COMPONENT

As shown in Fig. 1, we analyze the typical priors based on static and dynamic components of the video sequences, i.e., the temporal rank-1 property for video static component and the spatial-temporal smoothness and sparseness for video dynamic component. First, it is easy to observe that a video sequence can be regarded as the superposition of static and dynamic components from Figs. 1(a) (b) and (c). Second, Fig. 1(d) shows that the video background is temporally correlated, we introduce SVD on the matrix unfolding along the temporal dimension, the drastic decaying trend of the curve of the singular values statistics indicates the lower rank on the background component, i.e. stronger temporal correlation among the video background frames. As each frame of the video background possesses nearly the same information, and all background video frames can be linearly represented algebraically by any single frame, with its rank in temporal dimension approximately 1. Further, the quantitative accumulation energy ratio of top k normalized singular values is used to measure the close correlation along temporal domain of video background. Ideally, background frames possesses an exact replica, thus the ratio of top 1 the singular value is 1. Due to disturbance of noise and shadow, we find out only the top 1 singular values can achieve the ratio 0.9906, which justifies that the video background can be approximated as rank-1.

A great advantage of using the rank-1 constraint over the background prior is that it preserves the major information by minimizing the singular values of noise-dominant components except for the target rank. The nuclear norm constraint can obtain a solution that minimizes all singular values, but the physical meaning of singular values will be neglected. This will lead to the biased estimation of low-rank component. In contrast, the rank-1 regularization not only reserves the first singular value of a matrix, but also minimizes variables in residual rank which corresponds to minimizing the dynamic component of video data. From the above analysis of the rank-1 regularization based background prior, we only need to minimize the partial sum of singular values presented in the objective function [51], the corresponding mathematical formula is as follows

$$\|L\|_{r=1} = |rank(L) - 1| = \sum\nolimits_{i=2} \sigma_i(L) \tag{2}$$

where $\sigma_i(L)$ is the i^{th} singular value of the matrix L.

B. PROPERTY ANALYSIS AND MODELING DYNAMIC COMPONENT

For the sparse dynamic components E in video, it can be decomposed into smooth foreground and sparse noise: $E = X + S$ as shown in Figs. 1(c) (f) and (g). In Fig. 1(f), the moving car in video foreground is continuous among succeeding frames across temporal domain, moreover, the moving car of each frame is also smooth in local region across spatial domain. We term this prior as spatial-temporal continuity of video foreground, i.e., the regularization of smoothness on foreground can be achieved by imposing the anisotropic 3D total variation on X, which is defined in [36]– [39] as

$$\|X\|_{3D-TV} = \|DX\|_1 = \|D_h x\|_1 + \|D_v x\|_1 + \|D_t x\|_1 \tag{3}$$

where $x = vec(X)(vec(.)$ is the vectorization operator.). D_h, D_v and D_t are three difference operators along different dimension, and $D = [D_h, D_v, D_t]$. In Fig. 1(g), the fluttering leaves, shadow of car and possible camera noise are considered together as sparse noise S, and it is modeled by L_1 norm constraint.

C. PROPOSED TR1-RPCA-BASED BS MODEL

Based on the above analysis, we now integrate the BS problem into the following model

$$\begin{aligned} &\min_{X,L,E,S} \|L\|_{r=1} + \lambda^E\|E\|_1 + \lambda^S\|S\|_1 + \lambda^X\|DX\|_1, \\ &s.t.\ Y = L + E, \quad E = X + S \end{aligned} \tag{4}$$

where λ^E, λ^S and λ^X are the trade-off parameters. By introducing auxiliary variable M, Eq. (4) can be reformulated equivalently as follows

$$\begin{aligned} &\min_{X,L,E,S,M} \|L\|_{r=1} + \lambda^E\|E\|_1 + \lambda^S\|S\|_1 + \lambda^X\|M\|_1, \\ &s.t.\ Y = L + E, \quad E = X + S,\ M = DX \end{aligned} \tag{5}$$

This constrained problem (5) can be reformulated equivalently as following the augmented Lagrangian form:

$$\begin{aligned} &F_\mu(X, L, E, S, M, Z^Y, Z^E, Z^M) \\ &= \|L\|_{r=1} + \lambda^E\|E\|_1 + \left\langle Z^Y, Y-L-E\right\rangle + \frac{\mu}{2}\|Y-L-E\|_F^2 \\ &\quad + \lambda^S\|S\|_1 + \left\langle Z^E, E-X-S\right\rangle + \frac{\mu}{2}\|E-X-S\|_F^2 \\ &\quad + \lambda^X\|M\|_1 + \left\langle Z^M, M-DX\right\rangle + \frac{\mu}{2}\|M-DX\|_F^2 \end{aligned} \tag{6}$$

where Z^Y, Z^E and Z^M are the Lagrange multiplier vectors, and μ is a positive penalty scalar. Then we adopt the alternating direction method of multipliers (ADMM) [52] to solve Eq. (6) by alternatively minimizing following sub-problems:

(1) L sub-problem: we solve L by the following sub-problem:

$$L = \min_L \frac{\lambda^L}{\mu}\|L\|_{r=1} + \frac{1}{2}\left\|Y + \frac{1}{\mu}Z^Y - E - L\right\|_F^2 \tag{7}$$

The optimal solution of this sub-problem can be given by the partial singular value thresholding (PSVT) operator [51] as follows:

$$\begin{aligned} P_{1,\tau}[Y'] &= U_{Y'}(D_{Y1} + S_\tau[D_{Y2}])V_{Y'}^T \\ &= Y_1 + U_{Y2}S_\tau[D_{Y2}]V_{Y2}^T \end{aligned} \tag{8}$$

where $\tau = \mu\lambda^L$ and $Y' = Y + \mu^{-1}Z^Y - E$ can be regarded as the sum of two matrices, $Y' = Y_1 + Y_2 = U_{Y1}D_{Y1}V_{Y1}^T + U_{Y2}D_{Y2}V_{Y2}^T$, U_{Y1}, V_{Y1} are the singular vector matrices corresponding to the first singular value by SVD, and U_{Y2}, V_{Y2} are from the 2^{th} to the last singular values, $D_{Y1} = diag(\sigma_1, 0, \cdots, 0)$ and $D_{Y2} = diag(0, \sigma_2, \cdots, \sigma_t)$. And $S_\tau[x] = \text{sign}(x).\max(|x| - \tau, 0)$ is the soft-shrinkage operator [53].

(2) E sub-problem: we solve E by the following sub-problem:

$$\begin{aligned} E = \min_E \frac{\lambda^E}{\mu}\|E\|_1 &+ \frac{1}{2}\left\|Y + \frac{1}{\mu}Z^Y - E - L\right\|_F^2 \\ &+ \frac{1}{2}\left\|E + \frac{Z^E}{\mu} - X - S\right\|_F^2 \end{aligned} \tag{9}$$

This sub-problem can be solved by the popular soft shrinkage operator as follows:

$$E = S_{\lambda^E/\mu}[(Y + \frac{Z^Y}{\mu} - X - L) + (X + S - \frac{Z^E}{\mu})] \tag{10}$$

(3) X sub-problem: we solve X by the following sub-problem:

$$X = \min_X \frac{\mu}{2}\left\|E + \frac{Z^E}{\mu} - X - S\right\|_F^2 + \frac{\mu}{2}\left\|M + \frac{Z^M}{\mu} - DX\right\|_F^2 \tag{11}$$

Further, X can be solved by the following linear problem:

$$(\mu I + \mu D^*D)X = \mu(E - S) + Z^E + D^*(\mu M + Z^M) \tag{12}$$

where D^* the adjoint of D. Thanks to the block circulant structure of the matrix, it can be diagonalized by the 3D FFT matrix [54], then X can be efficiently and exactly solved like:

$$X = \mathcal{F}^{-1}\left(\frac{\mathcal{F}(\mu(E-S)+Z^E+D^*(\mu M+Z^M))}{\mu I+\mu(|\mathcal{F}(D_h)|^2+|\mathcal{F}(D_v)|^2+|\mathcal{F}(D_t)|^2)}\right) \quad (13)$$

(4) M sub-problem: we solve M by the following sub-problem:

$$M = \min_M \lambda^M \|M\|_1 + \frac{\mu}{2}\left\|M + \frac{Z^M}{\mu} - DX\right\|_F^2 \quad (14)$$

Just as the solving method of Eq. (9), its solution is as follows:

$$M = S_{\lambda^M/\mu}[DX - \frac{Z^M}{\mu}] \quad (15)$$

(5) S sub-problem: we solve S by the following sub-problem:

$$S = \min_S \frac{\lambda^S}{\mu}\|S\|_1 + \frac{1}{2}\left\|E + \frac{Z^E}{\mu} - X - S\right\|_F^2 \quad (16)$$

Like solving method of Eqs. (9) and (15), its solution is as follows:

$$S = S_{\lambda^S/\mu}[E + \frac{Z^E}{\mu} - X] \quad (17)$$

(6) Updating Multipliers: According to the ADMM, the corresponding multipliers are updated by the following form:

$$\begin{cases} Z^Y \leftarrow Z^Y + \mu(Y - L - E) \\ Z^E \leftarrow Z^E + \mu(E - X - S) \\ Z^M \leftarrow Z^M + \mu(M - DX) \end{cases} \quad (18)$$

where the penalty parameter μ follows an adaptive updating scheme.

D. PARAMETER SETTING

There are four parameters λ^E, λ^S, λ^X and μ in our model. For parameter λ^E, if it is too large, the trivial solution of $E = 0$ is obtained, otherwise small λ^E leads to $L = 0$. However, we have set $\lambda^E = 0.5/\sqrt{mn}$, similar to [10], because a strong rank-1 constraint is used on foreground component in our proposed model. Considering the different characteristics of background and foreground, we give different settings for λ^S and λ^X. Similar to the analysis of λ^E, when λ^S is very large, the solution of S is close to zero, otherwise small value generates to $X = 0$. For video frames with static background, the sparse components can be regarded as foreground, a large λ^S is beneficial to detect objects as well as to balance the parameter λ^E, and thus we set $\lambda^S = 4/\sqrt{mn}$ and $\lambda^X = 0.1/\sqrt{mn}$. But for video frames with dynamic background, the sparse components mainly include the foreground and disturbance just like a shadow or ripple. Therefore, we set a relative small λ^S to improve the separation of disturbance components, e.g., in *WaterSurface* with ripples we set $\lambda^S = 3.8/\sqrt{mn}$ and $\lambda^X = 0.2/\sqrt{mn}$, in blowing *Curtain* we set $\lambda^S = 3.5/\sqrt{mn}$ and $\lambda^X = 0.23/\sqrt{mn}$. For those scenes (*Video-2* and *library*) with relative big moving objects due to strong smoothness and sparseness of foreground, we set $\lambda^E = 0.1/\sqrt{mn}$, $\lambda^S = 3.9/\sqrt{mn}$ and $\lambda^X = 0.2/\sqrt{mn}$. Experimental results show that our settings is good. In all the experiments, μ is initialized by a small value $\mu = 1.25/C$ (C is the largest singular values of matrix Y) as suggested in [14] and [39], and then updated by the scheme:

$$\mu \leftarrow c\mu, \quad (19)$$

where c can be taken as 1.05.

For clarity, we summarize the whole procedure of optimization in **Algorithm 1**, and we abbreviate the proposed method as TR1-RPCA. The algorithm terminates when the maximal number of iteration is reached.

Algorithm 1 Optimization Algorithm for TR1-RPCA

Input: The measure Y

1: **Initialize:** $L = Y, X = S = M = E = 0, Z^Y = Z^E = Z^M = 0, \lambda^E, \lambda^S, \lambda^X$, and μ

2: **for** $k = 1, 2, \cdots K$ **do**
3: Updating L by Eq.(7);
4: Updating E by Eq.(9);
5: Updating X by Eq.(13);
6: Updating M by Eq.(15);
7: Updating S by Eq.(17);
8: Updating multipliers and the associated parameters by Eqs.(18) and (19);
9: **end for**

Output: Background L and foreground X

IV. EXPERIMENTAL RESULTS

In this section, we conduct experiments on synthetic and real video datasets to demonstrate the superiority of the proposed model, i.e., TR1-RPCA, over the existing state-of-the-art approaches for the BS task. And we use the F-measure to assess the detection performances of video foreground. F-measure is defined as:

$$F\text{-measure} = 2\frac{\text{precision.recall}}{\text{precision+recall}} \quad (20)$$

where recall and precision are defined as:

$$\text{recall} = \frac{\#\text{correctly classified foreground pixels}}{\#\text{foreground pixels in ground truth}} \quad (21)$$

$$\text{precision} = \frac{\#\text{correctly classified foreground pixels}}{\#\text{ pixels classified as foreground}} \quad (22)$$

The larger the F-measure is, the closer will be the detected foreground area to the ground truth foreground area. The comparison methods include four state-of-the-art RPCA methods: RPCA [10], MoG-RPCA [22], RegL1ALM [23], MoG [24], TVRPCA [39], ReProcs [47], MEDRoP [48] and incPCP [49] models.

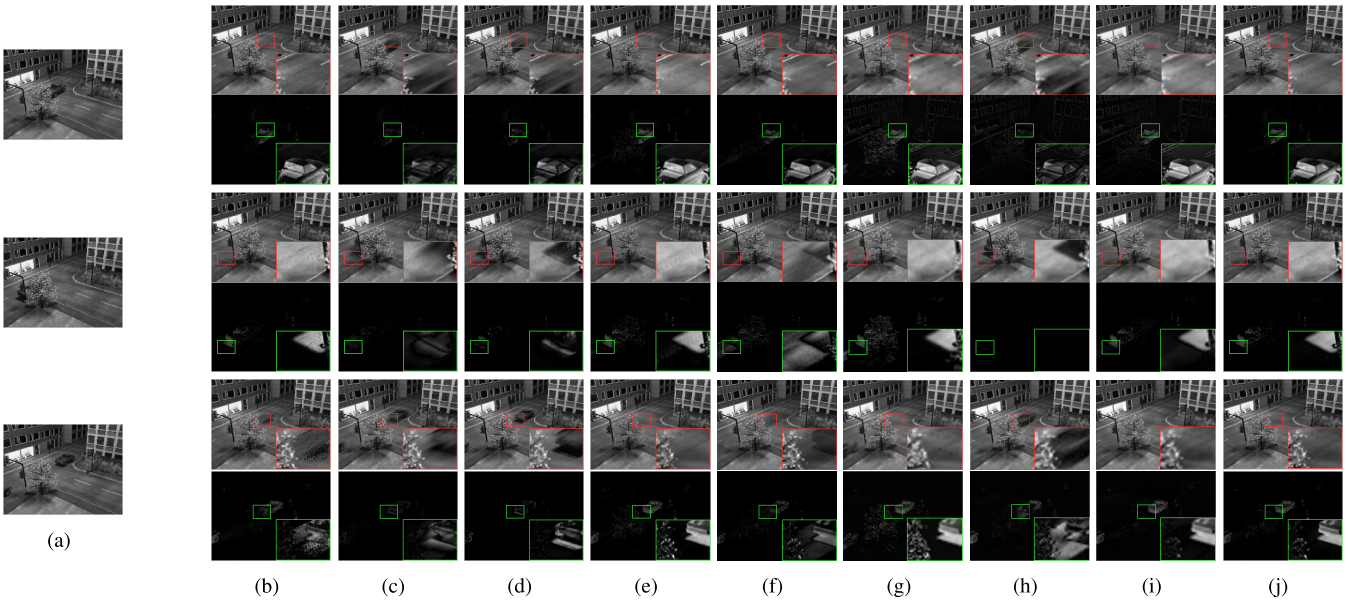

FIGURE 2. From left to right: (a) is original video frames, (b)-(j) are background and foreground frames extracted by different methods in synthetic data, i.e., (b) MoG-RPCA. (c) MoG. (d) RegL1ALM. (e) RPCA. (f) incPCP. (g) MEDRoP. (h) ReProcs. (i) TVRPCA. (j) TR1-RPCA.

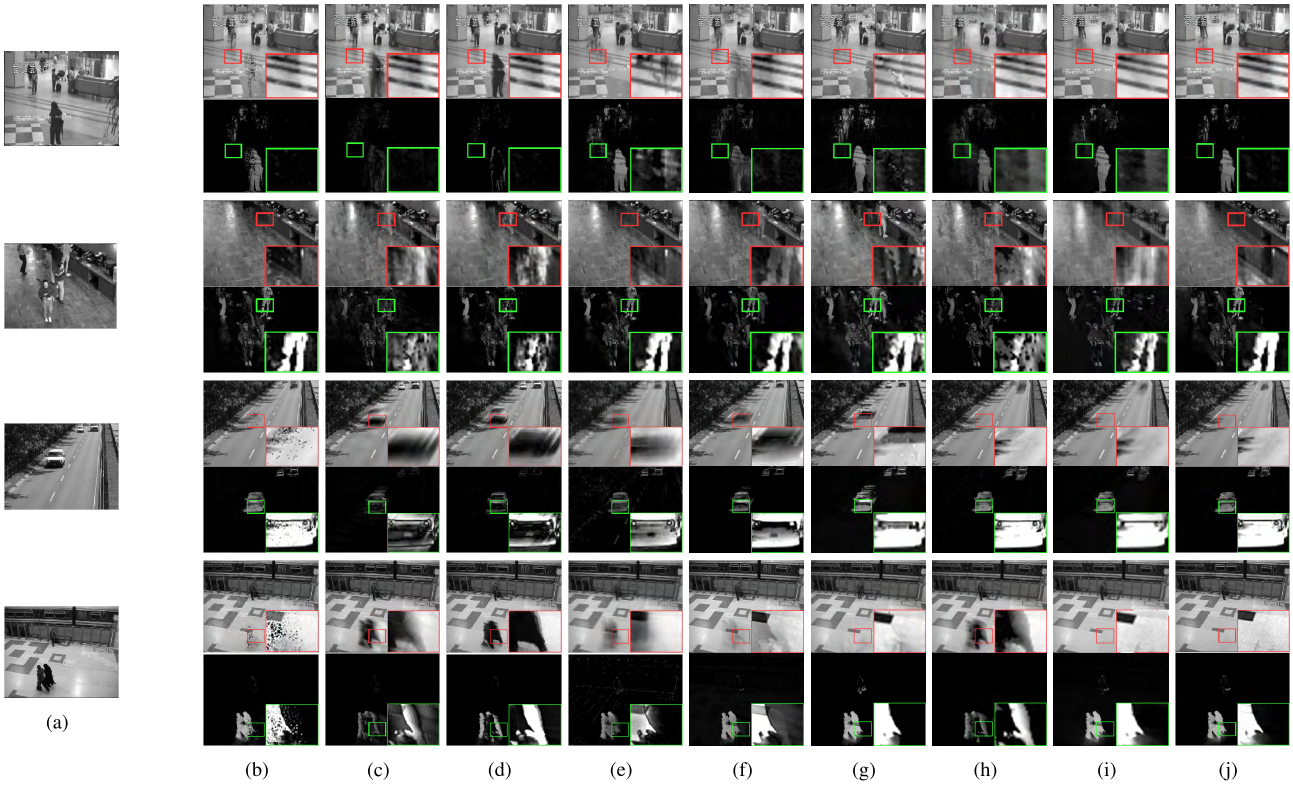

FIGURE 3. Visual results comparison on *Hall*, *Bootstrap*, *Highway* and *PETS* frames with static background: from left to right, (a) is original video frames, (b)-(j) are background and foreground frames extracted by different methods in real data, i.e., (b) MoG-RPCA. (c) MoG. (d) RegL1ALM. (e) RPCA. (f) incPCP. (g) MEDRoP. (h) ReProcs. (i) TVRPCA. (j) TR1-RPCA.

A. SYNTHETIC DATA

To evaluate the performance of our proposed approach, we select a bootstrap video of size $400\times300\times75$ with dynamic background on a synthetic SABS[1] dataset to conduct simulation experiments. The part of visual comparative results are shown in Fig. 2. From these figures, we find that the proposed TR1-RPCA method can estimate more clear background and accurate foreground, and avoid negative interference of the complexed background as much as possible. Comparatively, the results presented by MoG, incPCP and ReProcs cannot separate the background and foreground components completely, the undetected

[1] http://www.vis.uni-stuttgart.de/index.php?id=sabs.

FIGURE 4. Visual results comparison on *Watersurface* frames with dynamic background. The first and the last columns show the original frames and the corresponding annotated groundtruth foregrounds. The second to sixth columns show the foregrounds extracted by different methods in real data. (a) Original. (b) MoG-RPCA. (c) MoG. (d) RegL1ALM. (e) RPCA. (f) incPCP. (g) MEDRoP. (h) ReProcs. (i) TVRPCA. (j) TR1-RPCA. (k) Ground truth.

foreground information is mixed in the background, mainly because the compared methods have paid more attention to the dynamic components prior while neglecting the intrinsic known rank of the background. In MoG-RPCA model, the inaccurate estimation for the number of Gaussian distribution will lead to the underfitting to sparse foreground. The main goal of the RegL1ALM model is how to build an appropriate characterization form in matrix factorization framework for low-rank knowledge, thus its BS results are also unsatisfactory. The MEDRoP falsely detects the brightness changes and blowing leaves as the moving objects, and the TVRPCA over-smoothes the details and textures of moving objects. Although the RPCA method achieves relatively desirable moving object detection results, there are some artifacts in the background and some objects like fluttering leaves and the shadow of a car in the foreground are not as well detected as compared to the proposed TR1-RPCA.

B. REAL DATA

In this section, we collect the I2R,[2] UCSD[3] and CD.net[4] datasets, including 9, 5 and 4 video sequences respectively, to evaluate our proposed approach. These video sequences cover various kinds of background scenarios, such as static background (e.g., *Airport*, *Highway*, *Pedestrians*), dynamic background indoors (e.g., *Campus*, *Fountain*, *Escalator*, *Curtain*) and illumination changes (e.g., *Lobby*). For each video, we choose parts of frames with pre-annotated groundtruth foregrounds for evaluating the accuracy of foreground detection by all methods.

The results of typical frames with static background in the *Hall*, *Bootstrap*, *Highway* and *PETS* sequences are shown in Fig. 3. From the partial enlarged view of these figures, we can see that TR1-RPCA method can recover more perfect background with less ghost shadows and sharper foreground even under multi-object sequences. Comparatively, the results estimated by other competing methods falsely classify the static and dynamic components, and some objects originally belong to the static component are detected as the dynamic foreground. Table 1 lists the 18 quantitative comparative results based on F-measure, averaged on annotated groundtruth frames of each video in the known dataset. It is easy to observe the superiority of the proposed method to other competitive methods on all the tested videos.

The results of videos with dynamic background in the *Watersurface* and *Curtain* sequences are shown in Figs. 4 and 5. The proposed TR1-RPCA method can

[2]http://perception.i2r.a-star.edu.sg/bk model/bk index.html.

[3]http://www.svcl.ucsd.edu/projects/background/subtraction-ucsdbgsub-dataset.htm.

[4]http://wordpress-jodoin.dmi.usherb.ca/datasetOverview/.

TABLE 1. Quantitative performance comparison based the *F*-measure of different methods.

Datasets	Videos	MoG-RPCA	MoG	RegL1ALM	RPCA	incPCP	MEDRoP	ReProcs	TVRPCA	TR1-RPCA
I2R	Airport	0.4634	0.3957	0.1976	0.4800	0.1985	0.5026	0.3877	0.4086	**0.5467**
	ShoppingMall	0.6562	0.5745	0.1198	0.6654	0.1445	0.2579	0.4052	0.3178	**0.6804**
	Lobby	0.7442	0.7262	0.0408	0.7628	0.2763	0.6931	0.5375	0.5518	**0.7825**
	Escalator	0.5478	0.4644	0.1238	0.5478	0.2926	0.4154	0.3685	0.4431	**0.6297**
	Fountain	0.7977	0.4160	0.0883	0.8045	0.0403	0.5901	0.4944	0.7460	**0.8372**
	Campus	0.5041	0.3164	0.0205	0.4975	0.4943	0.3947	0.1889	0.5125	**0.5218**
	Hall	0.6708	0.5712	0.2633	0.6708	0.4553	0.5374	0.5829	0.4532	**0.7412**
	Curtain	0.6534	0.5350	0.1990	0.7538	0.3072	0.5610	0.5078	0.7911	**0.8122**
	WaterSurface	0.7744	0.3971	0.1449	0.8336	0.4892	0.6215	0.6973	0.8219	**0.9054**
UCSD	Freeway	0.2022	0.2083	0.0279	0.2123	0.1825	0.1062	0.1379	0.2018	**0.2365**
	Peds	0.2887	0.2715	0.0586	0.2712	0.2031	0.2610	0.2321	0.3219	**0.3751**
	Ocean	0.1859	0.1518	0.0218	0.1876	0.1108	0.1527	0.1639	0.1925	**0.2179**
	Rain	0.7753	0.6966	0.1444	0.7740	0.5163	0.6219	0.4217	0.7198	**0.7997**
	Traffic	0.3068	0.2401	0.0350	0.3015	0.2610	0.2100	0.1963	0.2995	**0.3239**
CD.net	Highway	0.4630	0.4201	0.1209	0.4750	0.4719	0.4417	0.4258	0.4517	**0.4922**
	Office	0.5961	0.5577	0.1188	0.7254	0.3029	0.7417	0.5297	0.6343	**0.7724**
	Pedestrians	0.8610	0.5683	0.0492	0.7721	0.1157	0.7875	0.7168	0.8057	**0.8872**
	PETS	0.8486	0.5073	0.0913	0.8612	0.5806	0.8657	0.5127	0.7704	**0.8779**

FIGURE 5. Visual results comparison on *Curtain* frames with dynamic background. The first and the last columns show the original frames and the corresponding annotated groundtruth foregrounds. The second to tenth columns show the foregrounds extracted by different methods in real data. (a) Original. (b) MoG-RPCA. (c) MoG. (d) RegL1ALM. (e) RPCA. (f) incPCP. (g) MEDRoP. (h) ReProcs. (i) TVRPCA. (j) TR1-RPCA. (k) Ground truth.

provide better object estimation with less noisy components when compared with ground truth foregrounds. While the MoG-RPCA, MoG RegL1ALM, incPCP and ReProcs approaches are only able to detect the profile of the dynamic objects, the RPCA, MEDRoP and TVRPCA confusedly embed the detected the dynamic objects of the adjacent

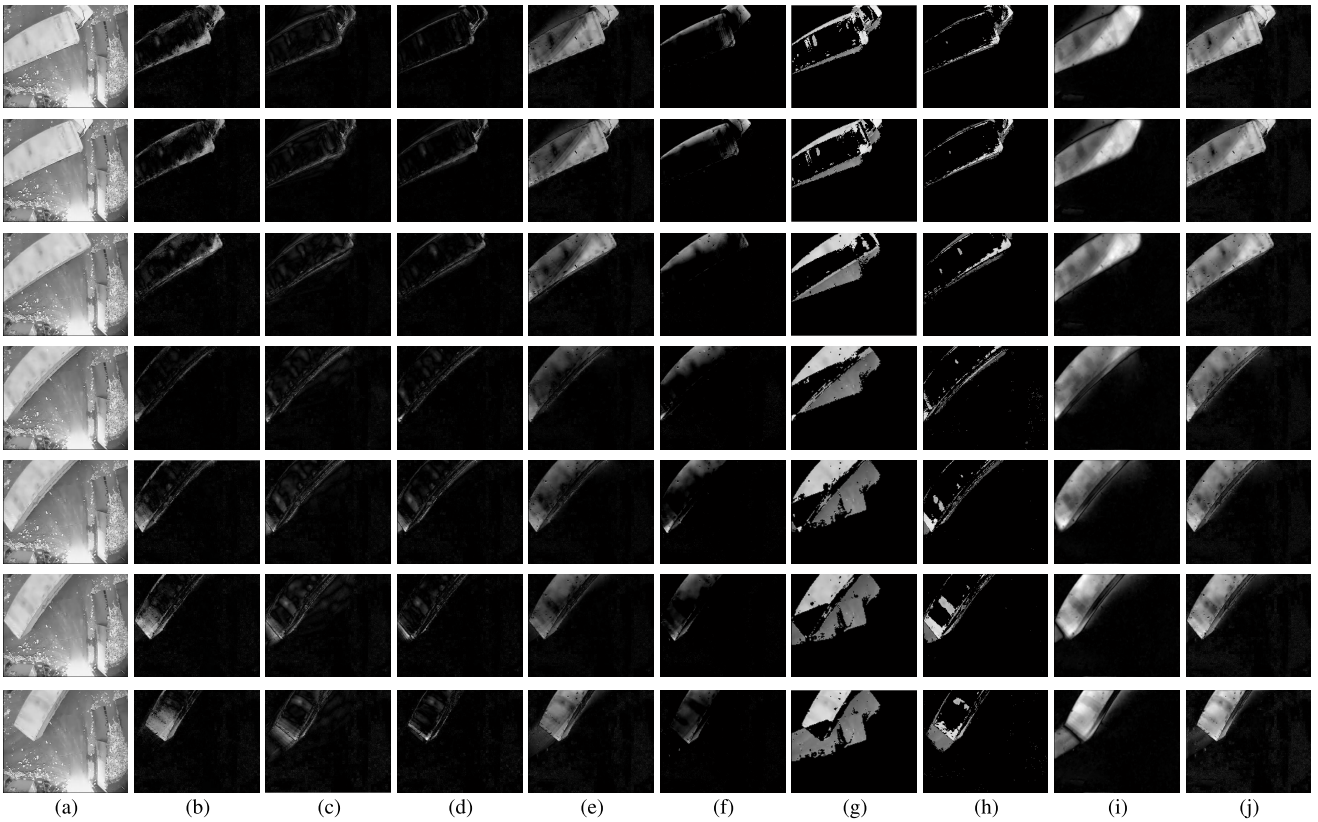

FIGURE 6. Visual results comparison on *Video-2* of BMC dataset. The first column show the original frames. The second to tenth columns show the foregrounds extracted by different methods in real data. (a) Original. (b) MoG-RPCA. (c) MoG. (d) RegL1ALM. (e) RPCA. (f) incPCP. (g) MEDRoP. (h) ReProcs. (i) TVRPCA. (j) TR1-RPCA.

frames into current foreground frame. It indicates that the spatial-temporal smoothness based on the TV regularizer can be more effective to characterize the slowly moving objects when compared with the sparseness prior of foreground video.

To further demonstrate the superior performance of TR1-RPCA in complex scenarios, we select two sequences: (1) *Video-2* from the BMC[5] dataset and (2) *library* captured by far-infrared camera on CD.net dataset. Different from the previous sequences, those moving objects of the two sequences are relatively big (close distance to the camera) and move slowly, which makes it more difficult to distinguish the static and dynamic components. The sequences and their corresponding results are presented in Figs. 7 and 8. The RPCA can produce relatively good results when those objects move in high speed, otherwise the foreground objects will generate severe artifacts and ghosting. The MoG-RPCA, MoG, RegL1ALM, incPCP and ReProcs can only detect the profile of moving objects, losing more textural details of the detected objects. The MEDRoP sharpens edges of video foreground while misses the slowly moving ingredient as shown in Fig. 8, and it sometimes confuses the dynamic objects of adjacent frames as shown in Fig. 7. The TRRPCA over-smoothes the details and falsely detects the dust behind the car as the moving objects (in Fig. 7). The results in Fig.8 show pseudo-shadows around the thermal objects and with that TR1-RPCA can correctly detect objects such as cars and pedestrians. In summary, the TR1-RPCA can correctly detect big objects with slow and continuous movements.

[5]http://bmc.iut-auvergne.com/.

C. EFFECTIVENESS ANALYSIS OF TV AND RANK-1 PRIORS

Here, we will use two experiments on watersurface to further demonstrate the effectiveness of TV and rank-1 regularization in our model. The first experiment is conducted via replacing the TV term by sparse prior, we denote it as SR1-RPCA for short. Another experiment is performed for BS task via replacing the rank-1 term by low-rank constraint based on nuclear norm, and it is abbreviated to TLR-RPCA.

Fig. 8 shows the visual results of SR1-RPCA, TLR-RPCA and the proposed TR1-RPCA methods algorithm on Watersurface. It is easy to observe that the results generated by SR1-RPCA have serious artifacts, with duplication of the standing person. TLR-RPCA regards the dynamic water ripples and static tree as the foreground components. By comparison, the proposed TR1-RPCA achieves the best BS results with consideration of more refined information in its configurations.

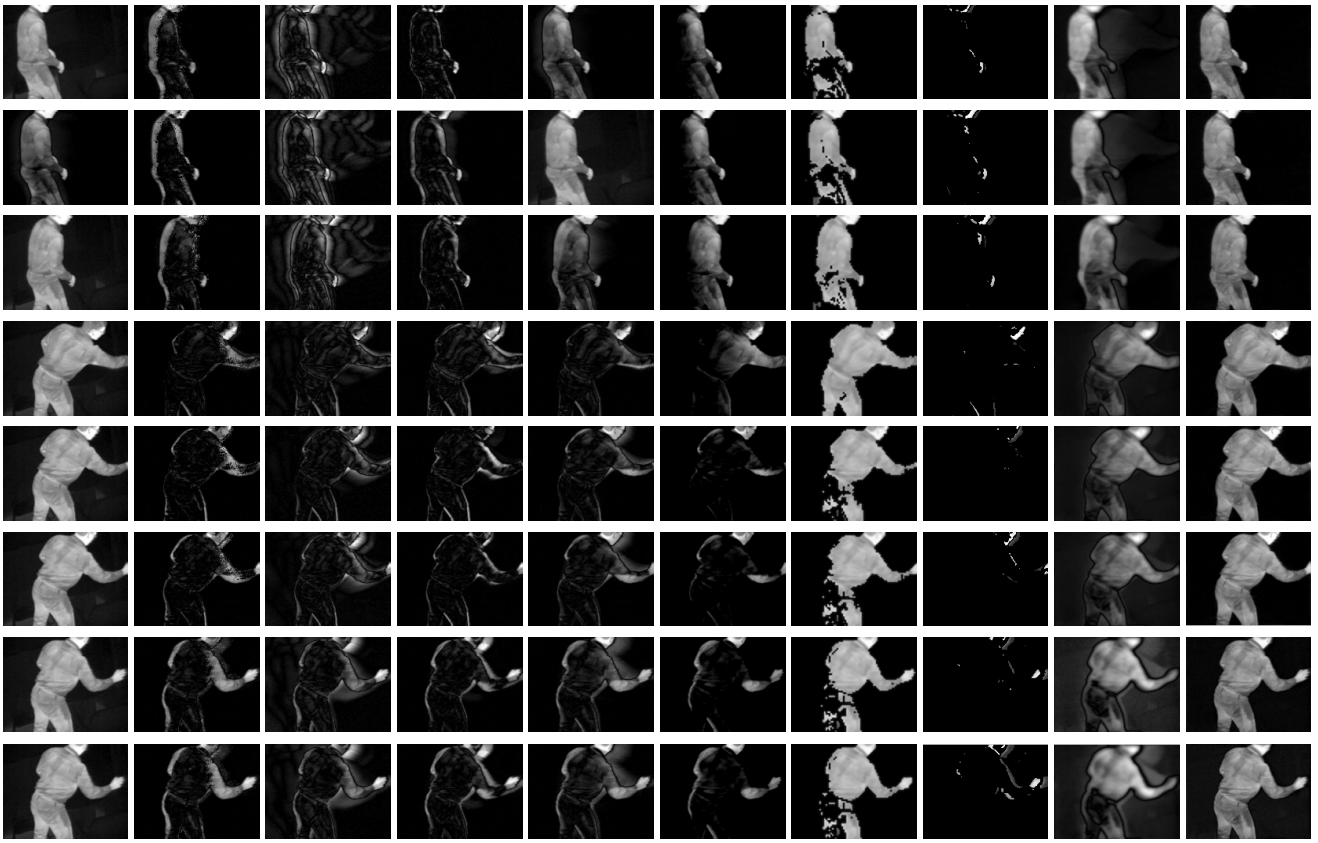

FIGURE 7. Visual results comparison on *library* by thermal camera on CD.net dataset. The first column show the original frames. The second to tenth columns show the foregrounds extracted by different methods in real data. (a) Original. (b) MoG-RPCA. (c) MoG. (d) RegL1ALM. (e) RPCA. (f) incPCP. (g) MEDRoP. (h) ReProcs. (i) TVRPCA. (j) TR1-RPCA.

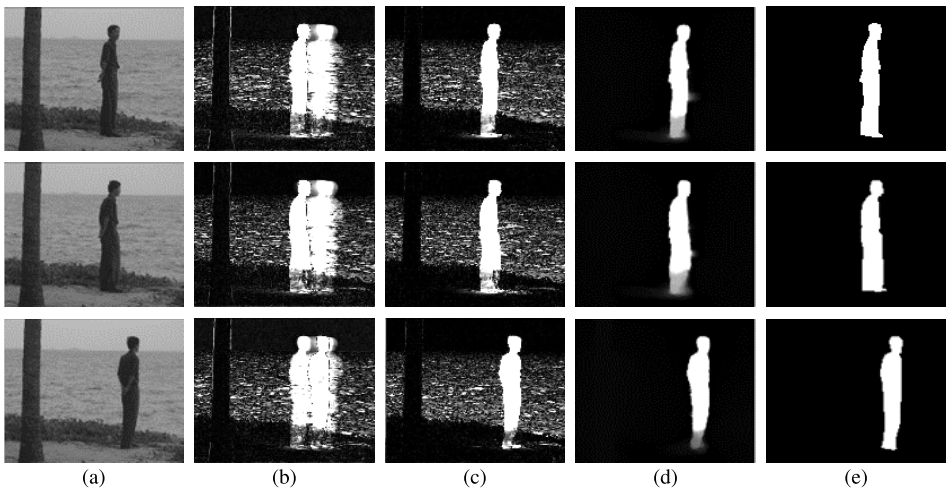

FIGURE 8. Visual results comparison of SR1-RPCA, TLR-RPCA and our TR1-RPCA methods on *Watersurface* frames with dynamic background. The first and the last columns show the original frames and the corresponding annotated groundtruth foregrounds. (a) Original. (b) SR1-RPCA. (c) TLR-RPCA. (d) TR1-RPCA. (e) Ground truth.

V. CONCLUSIONS

In this paper, we propose a joint TV and rank-1 regularized RPCA method for BS, in which more refined prior representations for the static and dynamic components of the video frames in RPCA framework are employed. The rank-1 property is employed to model the close temporal correlation

of the background (static component) in video frames, and the TV term and L_1 norm are used to model the spatial-temporal smoothness of dynamic foreground layer and sparseness of noise component. The extensive experiments on both synthetic and real datasets verify the superiority of TR1-RPCA approach, with noteworthy improvements over the state-of-the-art competing methods.

REFERENCES

[1] X. Zhou, C. Yang, and W. Yu, "Moving object detection by detecting contiguous outliers in the low-rank representation," *IEEE Trans. Pattern Anal. Mach. Intell.*, vol. 35, no. 3, pp. 597–610, Mar. 2013.

[2] C. Beleznai, B. Fruhstuck, and H. Bischof, "Multiple object tracking using local PCA," in *Proc. IEEE Int. Conf. Pattern Recognit.*, vol. 3, Aug. 2006, pp. 79–82.

[3] T. Bouwmans and E. H. Zahzah, "Robust PCA via principal component pursuit: A review for a comparative evaluation in video surveillance," *Comput. Vis. Image Understand.*, vol. 122, pp. 22–34, May 2014.

[4] H.-H. Lin, J.-H. Chuang, and T.-L. Liu, "Regularized background adaptation: A novel learning rate control scheme for Gaussian mixture modeling," *IEEE Trans. Image Process.*, vol. 20, no. 3, pp. 822–836, Mar. 2011.

[5] L. Li, W. Huang, I. Y.-H. Gu, and Q. Tian, "Statistical modeling of complex backgrounds for foreground object detection," *IEEE Trans. Image Process.*, vol. 13, no. 11, pp. 1459–1472, Nov. 2004.

[6] Y. Sheikh and M. Shah, "Bayesian modeling of dynamic scenes for object detection," *IEEE Trans. Pattern Anal. Mach. Intell.*, vol. 27, no. 11, pp. 1778–1792, Nov. 2005.

[7] J.-M. Guo, Y.-F. Liu, C.-H. Hsia, and C.-S. Hsu, "Hierarchical method for foreground detection using codebook model," *IEEE Trans. Circuits Syst. Video Technol.*, vol. 21, no. 6, pp. 804–815, Jun. 2011.

[8] L. Maddalena and A. Petrosino, "A self-organizing approach to background subtraction for visual surveillance applications," *IEEE Trans. Image Process.*, vol. 17, no. 7, pp. 1168–1177, Jul. 2008.

[9] L. Maddalena and A. Petrosino, "The SOBS algorithm: What are the limits?" in *Proc. IEEE Conf. Comput. Vis. Pattern Recognit. Workshops*, Jun. 2012, pp. 21–26.

[10] E. J. Candès, X. Li, Y. Ma, and J. Wright, "Robust principal component analysis?" *J. ACM*, vol. 58, no. 1, pp. 1–37, 2009.

[11] T. Bouwmans, A. Sobral, S. Javed, S. K. Jung, and E.-H. Zahzah, "Decomposition into Low-rank plus additive matrices for background/foreground separation: A review for a comparative evaluation with a large-scale dataset," *Comput. Sci. Rev.*, vol. 23, pp. 1–71, Feb. 2016.

[12] N. Vaswani, T. Bouwmans, S. Javed, and P. Narayanamurthy, "Robust subspace learning: Robust PCA, robust subspace tracking, and robust subspace recovery," *IEEE Signal Process. Mag.*, vol. 35, no. 4, pp. 32–55, Jul. 2018.

[13] J. Xue, Y. Zhao, W. Liao, and S. G. Kong, "Joint spatial and spectral low-rank regularization for hyperspectral image denoising," *IEEE Trans. Geosci. Remote Sens.*, vol. 56, no. 4, pp. 1940–1958, Apr. 2018.

[14] S. Gu, Q. Xie, D. Meng, W. Zuo, X. Feng, and L. Zhang, "Weighted nuclear norm minimization and its applications to low level vision," *Int. J. Comput. Vis.*, vol. 121, no. 2, pp. 183–208, Jan. 2017.

[15] Y. Xie, S. Gu, Y. Liu, W. Zuo, W. Zhang, and L. Zhang, "Weighted schatten *p*-norm minimization for image denoising and background subtraction," *IEEE Trans. Image Process.*, vol. 25, no. 10, pp. 4842–4857, Oct. 2016.

[16] F. Nie, H. Huang, and C. Ding, "Low-rank matrix recovery via efficient schatten p-norm minimization," in *Proc. 26th AAAI. Conf. Artif. Intell.*, 2012, pp. 655–661.

[17] K. Mohan and M. Fazel, "Iterative reweighted algorithms for matrix rank minimization," *J. Mach. Learn. Res.*, vol. 13, no. 1, pp. 3441–3473, 2012.

[18] Z. Kang, C. Peng, and Q. Cheng, "Robust PCA via nonconvex rank approximation," in *Proc. IEEE Int. Conf. Data Mining*, Nov. 2015, pp. 211–220.

[19] W. Dong, G. Shi, X. Li, Y. Ma, and F. Huang, "Compressive sensing via nonlocal low-rank regularization," *IEEE Trans. Image Process.*, vol. 23, no. 8, pp. 3618–3632, Aug. 2014.

[20] Q. Sun, S. Xiang, and J. Ye, "Robust principal component analysis via capped norms," in *Proc. IEEE 19th ACM SIGKDD Int. Conf. Knowl. Discovery Data Mining*, 2013, pp. 311–319.

[21] W. K. Leow, Y. Cheng, L. Zhang, T. Sim, and L. Foo, "Background recovery by fixed-rank robust principal component analysis," in *Proc. IEEE Int. Conf. Comput. Analys. Images Patterns*, 2013, pp. 54–61.

[22] Q. Zhao, D. Meng, Z. Xu, W. Zuo, and L. Zhang, "Robust principal component analysis with complex noise," in *Proc. Int. Conf. Mach. Learn.*, 2014, pp. 55–63.

[23] Y. Zheng, G. Liu, S. Sugimoto, S. Yan, and M. Okutomi, "Practical low-rank matrix approximation under robust L1-norm," in *Proc. IEEE Int. Conf. Pattern Recognit.*, Jun. 2012, pp. 1410–1417.

[24] D. Meng and F. De La Torre, "Robust matrix factorization with unknown noise," in *Proc. IEEE Int. Conf. Comput. Vis.*, Dec. 2013, pp. 1337–1344.

[25] H. Yong, D. Meng, W. Zuo, and L. Zhang, "Robust online matrix factorization for dynamic background subtraction," *IEEE Trans. Pattern Anal. Mach. Intell.*, vol. 40, no. 7, pp. 1726–1740, Jul. 2018.

[26] S. Wang, Y. Wang, Y. Chen, P. Pan, Z. Sun, and G. He, "Robust PCA using matrix factorization for background/foreground separation," *IEEE Access*, vol. 6, pp. 18945–18953, 2018.

[27] S. E. Ebadi and E. Izquierdo, "Foreground segmentation with tree-structured sparse RPCA," *IEEE Trans. Pattern Anal. Mach. Intell.*, vol. 40, no. 9, pp. 2273–2280, Sep. 2017.

[28] A. Sobral, T. Bouwmans, and E.-H. ZahZah, "Double-constrained RPCA based on saliency maps for foreground detection in automated maritime surveillance," in *Proc. IEEE Int. Conf. Adv. Video Signal Surveill.*, Aug. 2015, pp. 1–6.

[29] S. Javed, S. K. Jung, A. Mahmood, and T. Bouwmans, "Motion-aware graph regularized RPCA for background modeling of complex scenes," in *Proc. IEEE Int. Conf. Pattern Recognit.*, Dec. 2016, pp. 120–125.

[30] S. Javed, A. Mahmood, T. Bouwmans, and S. K. Jung, "Spatiotemporal low-rank modeling for complex scene background initialization," *IEEE Trans. Circuits Syst. Video Technol.*, vol. 28, no. 6, pp. 1315–1329, Jun. 2018.

[31] S. Javed, A. Mahmood, T. Bouwmans, and S. K. Jung, "Background–foreground modeling based on spatiotemporal sparse subspace clustering," *IEEE Trans. Image Process.*, vol. 26, no. 12, pp. 5840–5854, Dec. 2017.

[32] M. Xu, C. Li, H. Shi, J. Tang, and A. Zheng, "Moving object detection via integrating spatial compactness and appearance consistency in the low-rank representation," in *Proc. CCF China Conf. Comput. Vis.*, 2017, pp. 50–60.

[33] C. Guyon, T. Bouwmans, and E.-H. Zahzah, "Foreground detection via robust low rank matrix decomposition including spatio-temporal constraint," in *Proc. Asian. Conf. Comput. Vis.*, 2012, pp. 315–320.

[34] C. Guyon, T. Bouwmans, and E.-H. Zahzah, "Foreground detection via robust low rank matrix factorization including spatial constraint with Iterative reweighted regression," in *Proc. IEEE Int. Conf. Pattern Recognit.*, Nov. 2012, pp. 2805–2808.

[35] H. Woo and H. Park, "Robust asymmetric nonnegative matrix factorization," Dept. Comput. Appl. Math., University of California, Berkeley, Berkeley, CA, USA, Tech. Rep., Feb. 2014.

[36] X. Guo, X. Wang, L. Yang, X. Cao, and Y. Ma, "Robust foreground detection using smoothness and arbitrariness constraints," in *Proc. Eur. Conf. Comput. Vis.*, 2014, pp. 535–550.

[37] W. Cao *et al.*, "Total variation regularized tensor RPCA for background subtraction from compressive measurements," *IEEE Trans. Image Process.*, vol. 25, no. 9, pp. 4075–4090, Sep. 2016.

[38] S. Xia, H. Sun, and B. Chen, "A regularized tensor decomposition method with adaptive rank adjustment for Compressed-Sensed-Domain background subtraction," *Signal Process. Image Commun.*, vol. 62, pp. 149–163, Mar. 2018.

[39] X. Cao, L. Yang, and X. Guo, "Total variation regularized RPCA for irregularly moving object detection under dynamic background," *IEEE Trans. Cybern.*, vol. 46, no. 4, pp. 1014–1027, Apr. 2016.

[40] G. Pope, M. Baumann, C. Studer, and G. Durisi, "Real-time principal component pursuit," in *Proc. IEEE Asilomar Conf. Signals Syst. Comput.*, Nov. 2011, pp. 1433–1437.

[41] C. Qiu and N. Vaswani, "Real-time robust principal components' pursuit," in *Proc. Proc. IEEE Annu. Allerton Conf. Commun. Control Comput.*, Sep./Oct. 2010, pp. 591–598.

[42] X. Guo and X. Cao, "Speeding uplow rank matrix recovery for foreground separation in surveillance videos," in *Proc. IEEE Int. Conf. Multimedia Expo*, Jul. 2014, pp. 1–6.

[43] M. Anderson, G. Ballard, J. Demmel, and K. Keutzer, "Communication-avoiding QR decomposition for GPUs," in *Proc. IEEE Int. Parallel Distrib. Process. Symp.*, May 2011, pp. 48–58.

[44] N. Wang, T. Yao, J. Wang, and D.-Y. Yeung, "A probabilistic approach to robust matrix factorization," in *Proc. Eur. Conf. Comput. Vis.*, 2012, pp. 126–139.
[45] J. He, L. Balzano, and A. Szlam, "Incremental gradient on the Grassmannian for online foreground and background separation in subsampled video," in *Proc. IEEE. Conf. Comput. Vis. Pattern Recognit.*, Jun. 2012, pp. 1568–1575.
[46] J. Xu, V. K. Ithapu, L. Mukherjee, J. M. Rehg, and V. Singh, "GOSUS: Grassmannian online subspace updates with structured-sparsity," in *Proc. IEEE Int. Conf. Comput. Vis.*, Dec. 2013, pp. 3376–3383.
[47] H. Guo, C. Qiu, and N. Vaswani, "An online algorithm for separating sparse and low-dimensional signal sequences from their sum," *IEEE Trans. Signal Process.*, vol. 62, no. 16, pp. 4284–4297, Aug. 2014.
[48] P. Narayanamurthy and N. Vaswani. (2017). "Medrop: Memory-efficient dynamic robust PCA." [Online]. Available: https://arxiv.org/abs/1712.06061
[49] P. Rodriguez and B. Wohlberg, "Incremental principal component pursuit for video background modeling," *J. Math. Imag. Vis.*, vol. 55, no. 1, pp. 1–18, 2016.
[50] P. Rodríguez and B. Wohlberg, "A MATLAB implementation of a fast incremental principal component pursuit algorithm for video background modeling," in *Proc. IEEE Int. Conf. Image Process.*, Oct. 2014, pp. 3414–3416.
[51] T.-H. Oh, Y.-W. Tai, J.-C. Bazin, H. Kim, and I. S. Kweon, "Partial sum minimization of singular values in robust PCA: Algorithm and applications," *IEEE Trans. Pattern Anal. Mach. Intell.*, vol. 38, no. 4, pp. 744–758, Apr. 2016.
[52] S. Boyd, N. Parikh, E. Chu, B. Peleato, and J. Eckstein, "Distributed optimization and statistical learning via the alternating direction method of multipliers," *Found. Trends Mach. Learn.*, vol. 3, no. 1, pp. 1–122, Jan. 2011.
[53] E. T. Hale, W. Yin, and Y. Zhang, "Fixed-point continuation for ℓ_1-minimization: Methodology and convergence," *SIAM J. Optim.*, vol. 19, no. 3, pp. 1107–1130, 2008.
[54] M. Tao, J. Yang, and B. He, "Alternating direction algorithms for total variation deconvolution in image reconstruction," Dept. Math., Nanjing Univ. Nanjing, China, Tech. Rep. TR0918, 2009.

JIZE XUE received the B.S. degree in mathematics and applied mathematics from Shanxi Datong University, Datong, China, in 2014, and the M.S. degree in control engineering from Northwestern Polytechnic University, Xi'an, China, in 2017, where he is currently pursuing the Ph.D. degree with the School of Automation. His research interests include hyperspectral image processing, tensor completion, and pattern recognition.

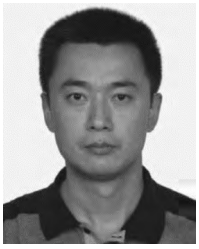

YONGQIANG ZHAO (M'05) received the B.S., M.S., and Ph.D. degrees in control science and engineering from Northwestern Polytechnic University, Xi'an, China, in 1998, 2001, and 2004, respectively. From 2007 to 2009, he was a Post-Doctoral Researcher at McMaster University, Hamilton, ON, Canada, and Temple University, Philadelphia, PA, USA, respectively. He is currently a Professor with Northwestern Polytechnical University. His research interests include polarization vision, hyperspectral imaging, compressive sensing, and pattern recognition.

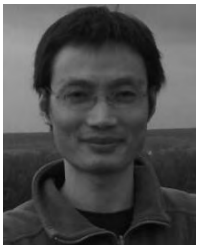

WENZHI LIAO (S'10–M'14–SM'16) received the B.S. degree in mathematics from Hainan Normal University, Haikou, China, in 2006, the Ph.D. degree in engineering from the South China University of Technology, Guangzhou, China, in 2012, and the second Ph.D. degree in computer science engineering from Ghent University, Ghent, Belgium, in 2012. Since 2012, he has been holding the post-doctoral position at Ghent University and as a Post-Doctoral Fellow with the Fund for Scientific Research, Flanders-FWO. His current research interests include pattern recognition, remote sensing, and image processing. In particular, his interests include mathematical morphology, multitask feature learning, multisensor data fusion, and hyperspectral image restoration. He is a member of the Geoscience and Remote Sensing Society and the IEEE GRSS Data Fusion Technical Committee. He received the Best Paper Challenge Awards on both the 2013 IEEE GRSS Data Fusion Contest and the 2014 IEEE GRSS Data Fusion Contest.

JONATHAN CHEUNG-WAI CHAN received the Ph.D. degree from The University of Hong Kong, Hong Kong, in 1999. From 1998 to 2001, he was with the Department of Geography, University of Maryland at College Park, College Park, MD, USA. From 2001 to 2005, he was with the Interuniversity Micro-Electronics Center, Leuven, Belgium. From 2005 to 2011, he was with the Department of Geography, Vrije Universiteit Brussel (VUB), Brussels, Belgium. From 2013 to 2014, he was a Marie Curie Fellow at the Fondazione Edmund Mach, Trentino, Italy. He is currently a Guest Professor with the Department of Electronics and Informatics, VUB. He is also a Visiting Professor with the Warsaw University of Life Sciences, Warsaw, Poland, and with Northwestern Polytechnical University, Xi'an, China. He was a Guest Editor of *Remote Sensing*, for the special issue on Spatial Enhancement of Hyperspectral Data and Applications.